

# Berkeley Supernova Ia Program V: Late-Time Spectra of Type Ia Supernovae

Jeffrey M. Silverman,<sup>1,2\*</sup> Mohan Ganeshalingam,<sup>1,3</sup> Alexei V. Filippenko<sup>1</sup>

<sup>1</sup>*Department of Astronomy, University of California, Berkeley, CA 94720-3411, USA*

<sup>2</sup>*Department of Astronomy, University of Texas, Austin, TX 78712-0259, USA*

<sup>3</sup>*Lawrence Berkeley National Laboratory, Berkeley, CA 94720, USA*

Accepted . Received ; in original form

## ABSTRACT

In this work we analyse late-time ( $t > 100$  d) optical spectra of low-redshift ( $z < 0.1$ ) Type Ia supernovae (SNe Ia) which come mostly from the Berkeley Supernova Ia Program dataset. We also present spectra of SN 2011by for the first time. The BSNIP sample studied consists of 34 SNe Ia with 60 nebular spectra, to which we add nebular spectral feature measurements of 20 SNe Ia from previously published work (Maeda et al. 2011; Blondin et al. 2012), representing the largest set of late-time SN Ia spectra ever analysed. The full width at half-maximum intensity (FWHM) and velocities of the [Fe III]  $\lambda 4701$ , [Fe II]  $\lambda 7155$ , and [Ni II]  $\lambda 7378$  emission features are measured in most observations of spectroscopically normal objects where the data have signal-to-noise ratios  $\gtrsim 20$  px<sup>-1</sup> and are older than 160 d past maximum brightness. The velocities of all three features are seen to be relatively constant with time, increasing only a few to  $\sim 20$  km s<sup>-1</sup> d<sup>-1</sup>. The nebular velocity ( $v_{\text{neb}}$ , calculated by taking the average of the [Fe II]  $\lambda 7155$  and [Ni II]  $\lambda 7378$  velocities) is correlated with the near-maximum-brightness velocity gradient and early-time ejecta velocity. Nearly all high velocity gradient objects have redshifted nebular lines while most low velocity gradient objects have blueshifted nebular lines. No correlation is found between  $v_{\text{neb}}$  and  $\Delta m_{15}(B)$ , and for a given light-curve shape there is a large range of observed nebular velocities. The data also indicate a correlation between observed  $(B - V)_{\text{max}}$  and  $v_{\text{neb}}$ .

**Key words:** methods: data analysis – techniques: spectroscopic – supernovae: general

## 1 INTRODUCTION

Type Ia supernovae (SNe Ia) can be used to accurately measure cosmological parameters (e.g., Astier et al. 2006; Riess et al. 2007; Wood-Vasey et al. 2007; Hicken et al. 2009; Kessler et al. 2009; Amanullah et al. 2010; Conley et al. 2011; Suzuki et al. 2012), and they led to the discovery of the accelerating expansion of the Universe (Riess et al. 1998; Perlmutter et al. 1999). SNe Ia are thought to be the result of thermonuclear explosions of C/O white dwarfs (WDs) (e.g., Hoyle & Fowler 1960; Colgate & McKee 1969; Nomoto et al. 1984; see Hillebrandt & Niemeyer 2000 for a review). Despite their cosmological utility, we are still missing a detailed understanding of the progenitor systems and explosion mechanisms (see Howell 2011, for further information).

By about 100 d past maximum brightness, SN Ia ejecta have expanded significantly and the SN enters the so-called “nebular phase” (as opposed to the “early-time” phase).

At these late epochs, SN Ia spectra consist of broad emission lines of (mostly) iron-group elements (IGEs) and can yield valuable insights into the physics of the explosion itself. However, SNe Ia often appear quite faint at these late phases and thus not many late-time spectra exist in the literature.

There are a handful of relatively “normal” SNe Ia (i.e., ones that follow the light-curve width versus luminosity relationship; Phillips 1993) that have published spectra at phases later than  $\sim 100$  d (e.g., Stritzinger & Sollerman 2007; Stanishev et al. 2007; Leloudas et al. 2009). In addition, there are some rare and peculiar SNe Ia with published late-time spectra (e.g., Jha et al. 2006; Silverman et al. 2011). While there are large spectroscopic samples of SNe Ia published (Matheson et al. 2008; Blondin et al. 2012; Silverman et al. 2012a), only a tiny fraction of those data consist of late-time spectra. However, moderate-sized comparative studies of  $\sim 14$ – $24$  SNe Ia with late-time spectra have been undertaken (Mazzali et al. 1998; Maeda et al. 2010a; Blondin et al. 2012).

\* E-mail: jsilverman@astro.as.utexas.edu

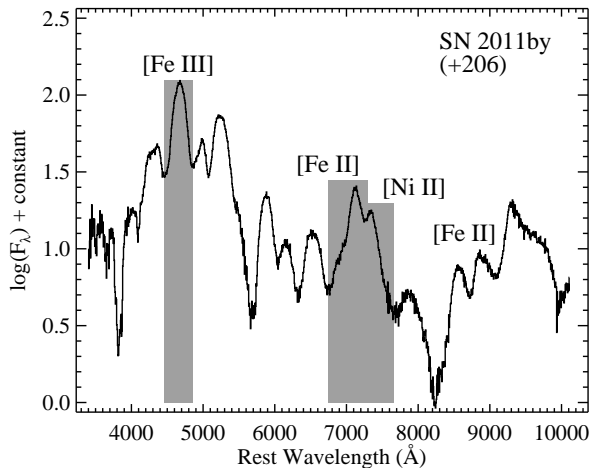


**Figure 1.** Spectrum of SN 2011by from 206 d past maximum brightness with prominent features labeled. The left-hand shaded area represents the [Fe III]  $\lambda$ 4701 feature while the right-hand shaded area represents the [Fe II]  $\lambda$ 7155 and [Ni II]  $\lambda$ 7378 features.

These works have concentrated mainly on three broad emission features centred near 4701, 7155, and 7378 Å (see Figure 1). The 4701 Å feature is likely a blend of various [Fe III] lines (Stritzinger et al. 2006; Maeda et al. 2010b) which come from material produced by a supersonic burning front (i.e., a detonation; Maeda et al. 2010a). On the other hand, the 7155 Å feature is likely due to [Fe II] (Maeda et al. 2010a) and the 7378 Å feature is probably from [Ni II] (Maeda et al. 2010b). These are both thought to trace material from where the explosion began and where the burning initially proceeded subsonically (i.e., a deflagration; Maeda et al. 2010a).

To the previous late-time SN Ia spectral studies we now add this work, where we analyse 60 nebular-phase ( $t > 100$  d) low-resolution optical spectra of 34 low-redshift ( $z < 0.1$ ) SNe Ia obtained as part of the Berkeley SN Ia Program (BSNIP; Silverman et al. 2012a). The data are presented by Silverman et al. (2012a) (supplemented herein with one new object: SN 2011by),<sup>1</sup> and we utilise spectral feature measurement tools similar to those described by Silverman et al. (2012d). The spectral data used in this work are summarised in Section 2, and our method of spectral feature measurement and our determination of nebular velocities are described in Section 3. Comparison of our late-time spectral measurements to other SN Ia observables can be found in Section 4. We present our conclusions in Section 5.

## 2 DATASET

The late-time spectral sample used in this work is a subset of spectra presented by Silverman et al. (2012a), with the addition of one new object (see Section 2.1). The majority of the spectra were obtained using the Shane 3 m telescope at

Lick Observatory with the Kast double spectrograph (Miller & Stone 1993) and the 10 m Keck telescopes with the Low Resolution Imaging Spectrometer (LRIS; Oke et al. 1995). The Kast data typically cover 3300–10,400 Å with resolutions of  $\sim 11$  and  $\sim 6$  Å on the red and blue sides (crossover wavelength  $\sim 5500$  Å), respectively. The LRIS spectra usually have a range of 3100–9200 Å with resolutions of  $\sim 7$  and  $\sim 5.5$  Å on the red and blue sides (crossover wavelength  $\sim 5600$  Å), respectively.

All data were reduced using standard reduction methods. For more information regarding the observations and data reduction, see Silverman et al. (2012a). The spectral ages of the BSNIP data referred to throughout this work are calculated using the redshift and Julian Date of maximum presented in Table 1 of Silverman et al. (2012a). Furthermore, photometric parameters (such as light-curve width and colour information) used in the present study can be found in Ganeshalingam et al. (2010).

The BSNIP sample contains 81 spectra of 43 SNe Ia older than 100 d past maximum brightness. In order to measure the three emission features mentioned above (i.e., [Fe III]  $\lambda$ 4701, [Fe II]  $\lambda$ 7155, and [Ni II]  $\lambda$ 7378), we required that the spectra span  $\sim 4300$ –7250 Å, which decreased the sample to 73 spectra of 38 SNe Ia. In previous BSNIP studies (Silverman et al. 2012d), we *a priori* ignored the extremely peculiar SN 2000cx (e.g., Li et al. 2001), SN 2002cx (e.g., Li et al. 2003; Jha et al. 2006), SN 2005gj (e.g., Aldering et al. 2006; Prieto et al. 2007), and SN 2005hk (e.g., Chornock et al. 2006; Phillips et al. 2007). These objects are so spectroscopically peculiar that it is difficult to consistently measure their spectral features in comparison to the bulk of the SN Ia population. Thus, in this work we will only concentrate on the SNe Ia that follow the “Phillips relation” (Phillips 1993) and can be used as cosmological distance indicators. We also include the underluminous SN 1991bg-like objects, which lie on a quadratic relationship between light-curve width and luminosity (e.g., Filippenko et al. 1992b; Leibundgut et al. 1993).

After removing the peculiar objects mentioned above, we are left with 33 SNe Ia with 58 BSNIP spectra having  $t > 100$  d. Of these, 7 were in the late-time sample studied by Maeda et al. (2010a), and those 7 plus 2 more were in the sample of Blondin et al. (2012). Each of the objects studied herein and the spectral phases are listed in Table 1, along with the full width at half-maximum intensity (FWHM) and velocity of the [Fe III]  $\lambda$ 4701 feature, and the velocities of the [Fe II]  $\lambda$ 7155 and [Ni II]  $\lambda$ 7378 features.

<sup>1</sup> All of the BSNIP data, along with the SN 2011by data, will be made public on 1 Jan. 2013 via the SuperNova DataBase (SNDB; Silverman et al. 2012a).

Table 1: Nebular feature measurements. All FWHMs and velocities are in  $\text{km s}^{-1}$ . Uncertainties are given in parentheses.

SN Name	Phase <sup>a</sup>	FWHM [Fe III] $\lambda 4701$	Velocity [Fe III] $\lambda 4701$	Velocity [Fe II] $\lambda 7155$	Velocity [Ni II] $\lambda 7378$	SN Name	Phase <sup>a</sup>	FWHM [Fe III] $\lambda 4701$	Velocity [Fe III] $\lambda 4701$	Velocity [Fe II] $\lambda 7155$	Velocity [Ni II] $\lambda 7378$
SN 1989M	146.8	15000 (900)	-2800 (160)	660 (40)	450 (30)	SN 2001ep	114.9	12400 (900)	-3370 (190)	...	...
SN 1991T	112.2	14300 (1500)	-2710 (130)	...	...	SN 2002bo	227.4	16600 (1300)	-1620 (80)	2330 (120)	2530 (200)
SN 1991T	318.4	17200 (1700)	810 (60)	...	...	SN 2002cs	119.0	15500 (1300)	-3810 (270)	...	...
SN 1991T	347.2	17000 (1400)	1810 (90)	...	...	SN 2002cs	143.5	15000 (1100)	-4280 (220)	...	...
SN 1991bg	161.9	3200 (300)	-1840 (110)	...	...	SN 2002cs	172.2	15800 (1600)	-3720 (220)	...	...
SN 1992G	110.8	14700 (1000)	-3000 (200)	...	...	SN 2002dp	103.1	14300 (1100)	-4080 (250)	...	...
SN 1992G	111.9	14700 (1000)	-3130 (260)	...	...	SN 2002dp	134.7	13800 (1200)	-2630 (120)	...	...
SN 1992G	126.8	16000 (1500)	-2990 (160)	...	...	SN 2002fk	148.7	14600 (1000)	-2650 (160)	-1370 (90)	-2750 (200)
SN 1993Z	112.5	15100 (1100)	-2120 (120)	...	...	SN 2003gs	199.5	14700 (1200)	-2630 (150)	3870 (260)	1210 (80)
SN 1993Z	132.4	15000 (1600)	-2120 (130)	...	...	SN 2004bv	135.2	14200 (1400)	-3300 (280)	...	...
SN 1993Z	144.3	14800 (1200)	-1230 (80)	...	...	SN 2004bv	161.7	14300 (1100)	-2530 (140)	...	...
SN 1993Z	161.2	14400 (1400)	-1350 (100)	1820 (100)	1180 (90)	SN 2004dt	109.2	13600 (1200)	-4970 (250)	...	...
SN 1993Z	200.8	15300 (1100)	-2880 (200)	1900 (150)	3660 (290)	SN 2004dt	168.9	...	...	-1470 (100)	-4220 (360)
SN 1993Z	232.7	14400 (900)	-720 (50)	1000 (60)	2390 (190)	SN 2005cf	317.1	15400 (1200)	-530 (20)	410 (40)	1400 (80)
SN 1994D	114.7	15400 (1100)	-3010 (170)	-2280 (150)	-1150 (100)	SN 2005ke	362.1	10500 (700)	-430 (30)	...	...
SN 1994ae	144.0	14500 (1200)	-2430 (140)	...	...	SN 2006D	126.5	14200 (1000)	-3320 (200)	...	...
SN 1994ae	218.6	12200 (900)	-890 (60)	...	...	SN 2006X	126.3	15200 (1400)	-2970 (160)	3420 (230)	2320 (160)
SN 1998bp	139.4	8700 (600)	-3490 (220)	...	...	SN 2006X	275.9	19300 (1400)	1210 (70)	2610 (170)	2730 (220)
SN 1998bp	163.1	10600 (500)	-2340 (150)	...	...	SN 2006X	358.4	23700 (2500)	-3290 (190)	1960 (140)	3180 (200)
SN 1998bu	235.1	15600 (1300)	-1030 (50)	-1890 (150)	-790 (60)	SN 2007af	113.8	13300 (1200)	-2920 (140)	...	...
SN 1998bu	279.0	16400 (1100)	-2040 (140)	-1710 (150)	-1430 (110)	SN 2007af	121.7	13300 (1300)	-2790 (190)	...	...
SN 1998bu	338.7	22200 (1900)	-650 (40)	-2640 (200)	-2330 (220)	SN 2007af	144.6	13100 (1100)	-3170 (200)	...	...
SN 1998es	106.0	13500 (1300)	-3790 (260)	...	...	SN 2007af	158.5	13600 (1300)	-3550 (210)	...	...
SN 1999aa	255.9	16700 (1500)	-1030 (60)	830 (40)	690 (50)	SN 2007fb	100.9	13700 (1300)	-3590 (240)	...	...
SN 1999aa	281.5	18500 (1500)	520 (30)	...	...	SN 2007gi	153.3	15800 (1400)	-1440 (90)	...	...
SN 1999ac	116.9	10300 (800)	-2200 (120)	...	...	SN 2007le	304.7	16700 (1600)	-230 (10)	2160 (150)	1890 (160)
SN 1999by	183.5	9500 (700)	-1440 (100)	...	...	SN 2007sr	135.7	13700 (1200)	-2280 (110)	...	...
SN 1999cw	104.6	14400 (1400)	-2920 (170)	...	...	SN 2008Q	199.3	15700 (1400)	-1860 (90)	-2940 (270)	-1450 (120)
SN 1999cw	132.1	13600 (900)	-2410 (150)	...	...	SN 2011by	206.1	14500 (1300)	-2260 (120)	-1350 (100)	-1470 (120)
SN 1999gh	118.0	12200 (1100)	-4200 (260)	1290 (90)	1840 (130)	SN 2011by	309.7	15300 (1200)	-280 (20)	-1210 (70)	-1750 (150)

<sup>a</sup>Phases of spectra are in rest-frame days relative to  $B$ -band maximum brightness using the heliocentric redshift and photometry reference presented in Table 1 of Silverman et al. (2012a) and Section 2.1 for SN 2011by.

## 2.1 SN 2011by

To the BSNIP sample discussed above we also add new data for the nearby Type Ia SN 2011by (see Appendix A for more information). We obtained broad-band *BVRI* photometry as well as 7 near-maximum-brightness spectra and 2 late-time spectra of SN 2011by. All of these data indicate that SN 2011by is photometrically ( $\Delta m_{15}(B) = 1.14 \pm 0.03$  mag) and spectroscopically normal.

SN 2011by will serve as a high-quality individual case study that can be directly compared to the larger late-time BSNIP sample discussed above. Adding this object and its two late-time spectra to the aforementioned dataset yields a sample of 60 spectra of 34 SNe Ia with  $t > 100$  d past maximum brightness. This represents one of the largest sets of late-time SN Ia spectra ever analysed.

## 3 MEASURING NEBULAR SPECTRAL FEATURES

The algorithm used in this work to measure the [Fe III]  $\lambda 4701$ , [Fe II]  $\lambda 7155$ , and [Ni II]  $\lambda 7378$  emission features is similar to that used to measure absorption features in near-maximum-brightness BSNIP spectra. It is described in detail by Silverman et al. (2012d), but here we give a brief summary of the procedure. Each spectrum first has its host-galaxy recession velocity removed and is corrected for Galactic reddening (according to the values presented in Table 1 of Silverman et al. 2012a), and then is smoothed using a Savitzky-Golay smoothing filter (Savitzky & Golay 1964).

For each feature, a linear background is defined by connecting points on either side of the feature and then subtracting out that background flux level. A cubic spline is then fit to the smoothed data and the expansion velocity is calculated from the wavelength at which the spline fit reaches its maximum. This maximum is also used to measure the FWHM for the [Fe III]  $\lambda 4701$  feature.

[Fe III]  $\lambda 4701$  is usually the strongest feature in late-time SN Ia spectra and is often seen to be a single-peaked, distinct feature. On the other hand, [Fe II]  $\lambda 7155$  and [Ni II]  $\lambda 7378$  are found to be blended into either a single- or double-peaked broad emission feature. Any spectrum where the two features were severely blended with each other (or showed more than two peaks near the wavelengths of interest) did not have velocities measured for [Fe II]  $\lambda 7155$  and [Ni II]  $\lambda 7378$ . For the spectra that do show clearly double-peaked profiles, a cubic spline is again fit to the smoothed data and the expansion velocities are calculated from the wavelengths at which the spline fit reaches its maximum on either side of the local minimum (i.e., the point between the two peaks). The FWHM and velocity of the [Fe III]  $\lambda 4701$  feature and the velocities of the [Fe II]  $\lambda 7155$  and [Ni II]  $\lambda 7378$  features are displayed in Table 1.

While we were able to measure [Fe III]  $\lambda 4701$  in all late-time spectra presented herein whose wavelength range included this feature, we were only able to accurately measure the velocities of [Fe II]  $\lambda 7155$  and [Ni II]  $\lambda 7378$  in 22 spectra of 15 SNe Ia (nebular velocities of 6 of these objects have been calculated previously; Maeda et al. 2010a; Blondin et al. 2012). In these previous studies, velocities were reported even when there was only a single peak near

these wavelengths. With only one peak, however, it is not clear which reference wavelength to use when calculating a nebular velocity, and so for a velocity measurement in this work we require that exactly two peaks be present in a late-time spectrum.

The underluminous SN 1991bg-like objects (e.g., Filippenko et al. 1992b; Leibundgut et al. 1993) have narrower emission profiles than do normal SNe Ia at late times, but they do not typically show the [Fe II]  $\lambda 7155$  and [Ni II]  $\lambda 7378$  features. Furthermore, the SN 1991T-like objects (e.g., Filippenko et al. 1992a; Phillips et al. 1992) and SN 1999aa-like objects (e.g., Li et al. 2001; Strolger et al. 2002; Garavini et al. 2004), which together generally represent overluminous SNe Ia, often have complex and multi-peaked profiles near 7300 Å, and thus we are again unable to accurately measure the velocities of [Fe II]  $\lambda 7155$  and [Ni II]  $\lambda 7378$  for most of these objects. We are, however, able to measure velocities in one spectrum of SN 1999aa. Note that Maeda et al. (2010a) cut these peculiar objects from their sample as well. Of the remaining “normal” SNe Ia, 6 of the spectra in which we are unable to reliably measure these features have low signal-to-noise ratios ( $S/N \lesssim 20 \text{ px}^{-1}$ ), with 3 of those having  $S/N < 5 \text{ px}^{-1}$ , and all normal SN Ia spectra with  $S/N > 20 \text{ px}^{-1}$  were successfully measured.

Even after removing 9 spectra of peculiar SNe Ia and 6 spectra with low  $S/N$ , there are still 23 instances where we are unable to measure reliable velocities for the [Fe II]  $\lambda 7155$  and [Ni II]  $\lambda 7378$  features. Nearly all of these failures are due to the spectra being obtained at too young a phase. Figure 2 shows a histogram of the ages of the spectra investigated in this work, *after* removing peculiar objects and low- $S/N$  spectra. The grey histogram represents the ages of spectra in which we are unable to measure [Fe II]  $\lambda 7155$  and [Ni II]  $\lambda 7378$  velocities, while the white histogram represents ages where we successfully measure the velocities. At epochs less than  $\sim 160$  d past maximum brightness, the emission near 7300 Å is often still multi-peaked and too complex to definitively identify the [Fe II]  $\lambda 7155$  and [Ni II]  $\lambda 7378$  features. Thus, in order to be able to measure these velocities, one should wait until  $\sim 160$  d past maximum, after which time we are able to measure the velocity in 16 of 17 spectra. Despite this finding, there *are* some BSNIP spectra at 115, 118, 126, 147, and 149 d past maximum that have measured velocities.

The oldest spectrum in our sample is from 362 d past maximum brightness, but it is SN 1991bg-like and we are unable to measure the velocities of the [Fe II]  $\lambda 7155$  and [Ni II]  $\lambda 7378$  features. The next-oldest spectrum is from 358 d past maximum and in that case we are able to measure the velocities accurately. Thus, the epoch range in which we successfully measure nebular velocities of [Fe II]  $\lambda 7155$  and [Ni II]  $\lambda 7378$  is 115–358 d past maximum, with the majority of the spectra in the range 160–358 d past maximum. Both Maeda et al. (2010a) and Blondin et al. (2012) had a similar range ( $\sim 150$ –400 d past maximum), with the vast majority of their spectra being older than  $\sim 200$  d past maximum.

### 3.1 Calculating Nebular Velocities

Following Maeda et al. (2010a) and Blondin et al. (2012), we calculate nebular velocities from the mean of the individual velocities of the [Fe II]  $\lambda 7155$  and [Ni II]  $\lambda 7378$  features.

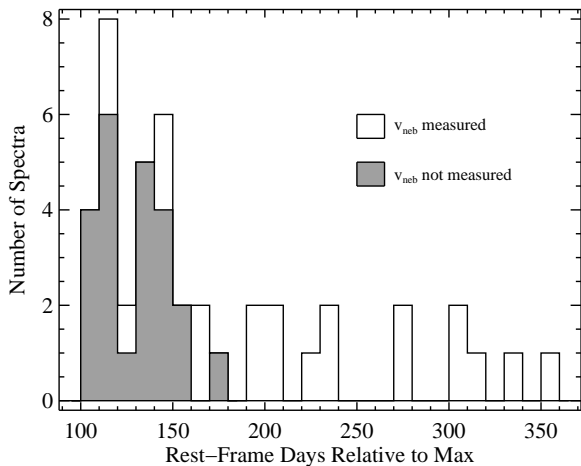


**Figure 2.** Histogram of spectral ages after removing peculiar objects and low-S/N spectra. The grey area represents spectra in which we are unable to measure [Fe II]  $\lambda 7155$  and [Ni II]  $\lambda 7378$  velocities. The white area represents spectra in which we can measure these velocities. Note that the vast majority of spectra with  $t > 160$  d have measured velocities.

Thus, the nebular velocity represents the typical velocity of material synthesized at the earliest times in the SN explosion. Previous studies used the difference between the two velocities as the uncertainty of the nebular velocity, but we use the difference divided by two (since that is how much the average differs from each measurement).

For the 4 SNe Ia in which we are able to measure both velocities in multiple late-time spectra, the nebular velocity is the average of all [Fe II]  $\lambda 7155$  and [Ni II]  $\lambda 7378$  velocities and the uncertainty is the average difference. The calculated nebular velocities ( $v_{\text{neb}}$ ) of all 15 SNe Ia with [Fe II]  $\lambda 7155$  and [Ni II]  $\lambda 7378$  velocity measurements are listed in the ninth column of Table 2, along with various classifications and other measured properties.

The second column of Table 2 gives the decline rate of the light curve,  $\Delta m_{15}(B)$ , and the third column shows the observed  $B-V$  colour of the SN at  $B$ -band maximum brightness,  $(B-V)_{\text{max}}$ , both taken from Ganeshalingam et al. (2010). Also displayed in the table is the velocity of the Si II  $\lambda 6355$  feature within 8 d of maximum brightness (fifth column) and a classification based on that velocity of either normal velocity or high velocity (fourth column; e.g., Wang et al. 2009). The rate of decrease of the expansion velocity, also known as the velocity gradient ( $\dot{v}$ , seventh column), and the velocity of the Si II  $\lambda 6355$  feature extrapolated to  $t = 0$  d using  $\dot{v}$  ( $v_0$ , eighth column) are also shown in Table 2 along with a classification based on  $\dot{v}$  (sixth column; e.g., Benetti et al. 2005). The tenth (eleventh) column of the table is the EW of narrow Na I D (Ca II H&K) absorption from the host galaxy of each SN (see Section 4.3.1 for more information on these measurements). Objects listed with a ‘†’ are part of the low-extinction sample (see Section 4.3.2). Note that while most of the measurements come directly from Silverman et al. (2012d), some of the near-maximum-light Si II  $\lambda 6355$  velocities were measured from data presented by Matheson et al. (2008) and Blondin et al. (2012).

The range of nebular velocities calculated in this study

is approximately  $\pm 2900$  km s $^{-1}$ , similar to the range found in previous work (Maeda et al. 2010a; Blondin et al. 2012). A comparison of the nebular velocities of the 6 SNe Ia that are found in the current sample as well as previous studies shows that the values calculated herein are consistent with previous work, with average absolute differences of a few hundred km s $^{-1}$  and no detectable bias (Maeda et al. 2010a, 2011; Blondin et al. 2012). The average uncertainty of  $v_{\text{neb}}$  (which is half the difference between the individual velocities of the [Fe II]  $\lambda 7155$  and [Ni II]  $\lambda 7378$  features) is  $\sim 490$  km s $^{-1}$ , slightly larger than the typical uncertainty in the measurements of Maeda et al. (2010a).

## 4 ANALYSIS

### 4.1 [Fe III] $\lambda 4701$

The FWHM of the [Fe III]  $\lambda 4701$  feature has been seen to possibly be anticorrelated with  $\Delta m_{15}(B)$  (Mazzali et al. 1998). In that work, both overluminous SN 1991T-like objects *and* underluminous SN 1991bg-like objects were found to follow the correlation. More recently, Blondin et al. (2012) found a similar result with a Pearson correlation coefficient of  $-0.71$  for all of their late-time data, but when their two underluminous SNe Ia were removed it decreased to  $-0.17$  (i.e., no correlation). This latter result was questioned, however, due to the fact that spectra at epochs earlier than 250–300 d past maximum brightness were used (Mazzali & Hachinger 2012).

Figure 3 shows the FWHM measurements of the [Fe III]  $\lambda 4701$  feature versus  $\Delta m_{15}(B)$  from the BSNIP spectra, as well as previously published values for 18 SNe (Maeda et al. 2011; Blondin et al. 2012). The shape of each data point signifies its ‘Benetti Type’ (based on  $\dot{v}$ ): squares are low velocity gradient (LVG) objects, triangles are high velocity gradient (HVG) objects, stars are FAINT objects, and circles are objects for which we are unable to determine a Benetti Type. The colour of each point represents its ‘Wang Type’ (based on Si II  $\lambda 6355$  velocity): blue is for normal-velocity objects, red is for HV objects, and black is objects for which we are unable to determine a Wang Type. Some of the outlying points are labeled with their object name.

As in previous studies (Mazzali et al. 1998; Blondin et al. 2012), the BSNIP data show that the FWHM of [Fe III]  $\lambda 4701$  is anticorrelated with  $\Delta m_{15}(B)$  (Pearson correlation coefficient of  $-0.66$ ) and the linear fit to all of the data is shown as the solid line in Figure 3. The slope of this line,  $-0.073$  mag/( $10^3$  km s $^{-1}$ ), is consistent with that of Blondin et al. (2012) but inconsistent with that of Mazzali et al. (1998), and the correlation is significant at the  $> 3\sigma$  level. If we remove only the underluminous SN 1991bg, the linear fit is nearly unchanged (the dashed line in the figure) and the correlation weakens only slightly (Pearson coefficient of  $-0.61$ ). If we instead remove the 8 objects with  $\Delta m_{15}(B) > 1.6$  mag (i.e., all of the underluminous objects in the dataset), the correlation effectively disappears (Pearson coefficient of  $-0.34$ ) and the slope of the linear fit (the dotted line in Figure 3) is consistent with 0 at the  $\sim 2\sigma$  level.

The findings of Blondin et al. (2012) confirmed above have recently been questioned due to their use of spectra at epochs earlier than 250–300 d past maximum brightness

**Table 2.** Summary of objects studied. Uncertainties are given in parentheses.

SN Name	$\Delta m_{15}(B)^a$ (mag)	$(B - V)_{\max}^a$ (mag)	Wang Type <sup>b</sup>	Si II $\lambda 6355$ Vel. <sup>c</sup> ( $10^3$ km s <sup>-1</sup> )	Benetti Type <sup>d</sup>	$v^e$ (km s <sup>-1</sup> d <sup>-1</sup> )	$v_0^f$ ( $10^3$ km s <sup>-1</sup> )	Nebular Vel. <sup>g</sup> (km s <sup>-1</sup> )	EW(Na) (Å)	EW(Ca) (Å)
SN 1989M	1.10 (0.20)	...	HV	12.46 (0.10)	HVG	291.84 (139.49)	13.19 (0.42)	560 (110)	1.88 (0.73)	0.36 (0.18)
SN 1993Z	...	...	...	...	...	...	...	1990 (630)	1.56 (0.40)	0.96 (1.67)
SN 1994D <sup>†</sup>	1.36 (0.05)	-0.053 (0.035)	N	10.72 (0.10)	LVG	33.43 (6.77)	10.60 (0.05)	-1720 (570)	0.40 (0.44)	0.09 (0.08)
SN 1998bu	1.05 (0.03)	0.292 (0.032)	N	10.84 (0.11) <sup>b</sup>	LVG <sup>b</sup>	46.52 (5.38) <sup>h</sup>	11.01 (0.05) <sup>h</sup>	-1800 (280)	1.52 (1.12)	0.39 (0.19)
SN 1999aa <sup>†</sup>	0.79 (0.05)	-0.093 (0.033)	...	10.50 (0.10)	LVG <sup>j</sup>	14.33 (3.52) <sup>j</sup>	10.49 (0.03) <sup>j</sup>	760 (70)	0.44 (0.64)	0.27 (0.14)
SN 1999gh <sup>†</sup>	1.69 (0.05)	0.190 (0.000)	N	11.02 (0.10)	FAINT	46.49 (10.13)	11.20 (0.13)	1570 (280)	0.50 (0.25)	...
SN 2002bo	1.15 (0.04)	0.315 (0.052)	HV	13.88 (0.10)	HVG	245.14 (8.12)	13.61 (0.09)	2430 (100)	2.36 (0.53)	0.57 (0.31)
SN 2002fk <sup>†</sup>	1.20 (0.03)	-0.155 (0.032)	N	9.51 (0.10)	LVG <sup>j</sup>	11.21 (8.28) <sup>j</sup>	9.74 (0.05) <sup>j</sup>	-2060 (690)	0.46 (0.09)	0.26 (0.07)
SN 2003gs	1.83 (0.02) <sup>k</sup>	0.634 (0.021) <sup>k</sup>	...	11.00 (0.20) <sup>k</sup>	...	...	...	2540 (1330)	0.98 (0.49)	...
SN 2004dt	1.29 (0.05)	-0.080 (0.034)	HV	14.34 (0.10)	HVG	269.45 (8.34)	14.70 (0.10)	-2850 (1380)	1.80 (1.04)	...
SN 2005cf <sup>†</sup>	1.08 (0.03)	-0.062 (0.031)	N	10.26 (0.10)	HVG	106.69 (149.59)	10.13 (0.25)	910 (500)	0.14 (0.09)	0.53 (0.26)
SN 2006X	1.10 (0.04)	1.260 (0.034)	HV	15.26 (0.10)	HVG <sup>j</sup>	184.80 (5.82) <sup>j</sup>	15.63 (0.06) <sup>j</sup>	2700 (410)	2.04 (1.61)	1.05 (0.46)
SN 2007le	1.02 (0.04)	0.280 (0.039)	HV	12.09 (0.10)	HVG	93.35 (12.65)	12.77 (0.18)	2030 (140)	2.36 (0.62)	0.33 (0.17)
SN 2008Q <sup>†</sup>	1.25 (0.08)	-0.012 (0.031)	HV	11.09 (0.10)	HVG <sup>j</sup>	82.66 (16.22) <sup>j</sup>	11.64 (0.05) <sup>j</sup>	-2200 (750)	0.44 (0.22)	...
SN 2011by	1.14 (0.03)	-0.061 (0.032)	N	10.35 (0.14)	LVG	52.83 (8.76)	10.40 (0.08)	-1450 (170)	0.66 (0.16)	0.47 (0.41)

<sup>†</sup>Object is part of the low-extinction sample (see text for details).

<sup>a</sup>Values taken from Ganeshalingam et al. (2010).

<sup>b</sup>Classification based on the velocity of the Si II  $\lambda 6355$  line near maximum brightness (Wang et al. 2009). ‘HV’ = high velocity; ‘N’ = normal. Taken from Silverman et al. (2012d).

<sup>c</sup>Velocity of the Si II  $\lambda 6355$  feature within 8 d of maximum brightness. Taken from Silverman et al. (2012d) unless otherwise noted.

<sup>d</sup>Classification based on the velocity gradient of the Si II  $\lambda 6355$  line (Benetti et al. 2005). ‘HVG’ = high velocity gradient; ‘LVG’ = low velocity gradient; ‘FAINT’ = faint/underluminous. Taken from Silverman et al. (2012d) unless otherwise noted.

<sup>e</sup>Change in velocity with time, near maximum brightness (i.e., the velocity gradient). Taken from Silverman et al. (2012d) unless otherwise noted.

<sup>f</sup>Velocity of the Si II  $\lambda 6355$  feature extrapolated to  $t = 0$  d based on the velocity gradient. Taken from Silverman et al. (2012d) unless otherwise noted.

<sup>g</sup>Average nebular velocity of the [Fe II]  $\lambda 7155$  and [Ni II]  $\lambda 7378$  features for all late-time spectra of a given object. The uncertainty is the average difference between the velocity of the two features.

<sup>h</sup>Si II  $\lambda 6355$  velocity, Benetti type, velocity gradient, and  $v_0$  measured from data presented by Matheson et al. (2008).

<sup>i</sup>Classification scheme only applies to spectroscopically normal SNe Ia.

<sup>j</sup>Benetti type, velocity gradient, and  $v_0$  measured from BSNIP data as well as data presented by Blondin et al. (2012).

<sup>k</sup> $\Delta m_{15}(B)$  and  $(B - V)_{\max}$  taken from Krisciunas et al. (2009). Si II  $\lambda 6355$  velocity taken from Suntzeff et al. (2003).

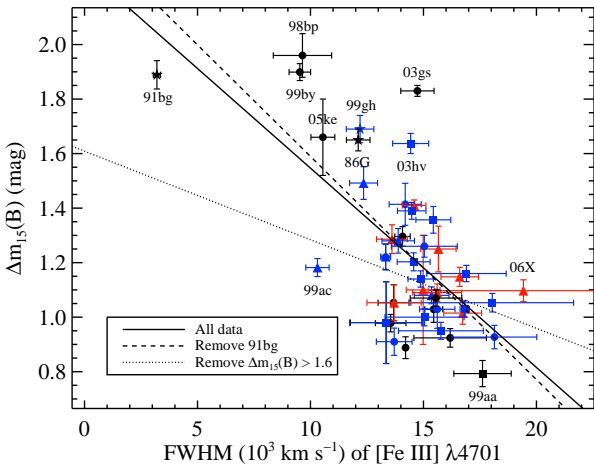


**Figure 3.** FWHM of [Fe III]  $\lambda 4701$  versus  $\Delta m_{15}(B)$  from BSNIP and 18 objects from Maeda et al. (2011) and Blondin et al. (2012). Squares are LVG objects, triangles are HVG objects, stars are FAINT objects, and circles are objects for which we are unable to determine a Benetti Type. Blue points are normal-velocity objects, red points are HV objects, and black points are objects for which we are unable to determine a Wang Type. Some of the outlying points are labeled. Linear fits to the data are also displayed: all data (solid), after removing SN 1991bg (dashed), and after removing all 6 objects with  $\Delta m_{15}(B) > 1.6$  mag (dotted).

(Mazzali & Hachinger 2012). To investigate this possibility, we performed a separate analysis of the FWHM of the [Fe III]  $\lambda 4701$  feature versus  $\Delta m_{15}(B)$  using only the oldest spectra from BSNIP, Maeda et al. (2011), and Blondin et al. (2012). There were 16 (8) objects with spectra obtained at  $t > 250$  d (300 d) past maximum brightness, and only a modest anticorrelation was found for these data with a Pearson coefficient of  $-0.55$  ( $-0.69$ ). When removing the 2 (1) underluminous objects with  $\Delta m_{15}(B) > 1.6$  mag having spectra at these latest epochs, the possible correlation completely disappears. Thus, it seems that at all epochs the possible relationship between the FWHM of the [Fe III]  $\lambda 4701$  feature and  $\Delta m_{15}(B)$  is being driven almost completely by the most underluminous SNe Ia, perhaps indicating the existence of two groups of points rather than a linear correlation.

Regarding the velocity of the [Fe III]  $\lambda 4701$  feature, Stritzinger et al. (2006) found no significant temporal change in their measurements and Maeda et al. (2010a) state that the feature shows “virtually no Doppler shift.” However, later work from the latter group show blueshifts of 2000–4500 km s<sup>-1</sup> for  $t < 200$  d, with the velocity steadily approaching 0 for  $t > 200$  d (Maeda et al. 2010b, 2011). This more recent result is also seen in the BSNIP data. In Figure 4 all measured velocities of [Fe III]  $\lambda 4701$  are plotted, with solid lines connecting multiple velocities of individual objects. Squares represent spectra for which we measured a nebular velocity, while  $\times$  symbols represent spectra for which we did not.

The overall trend (which matches what was found by Maeda et al. 2010b) is clear: velocities are blueshifted typi-

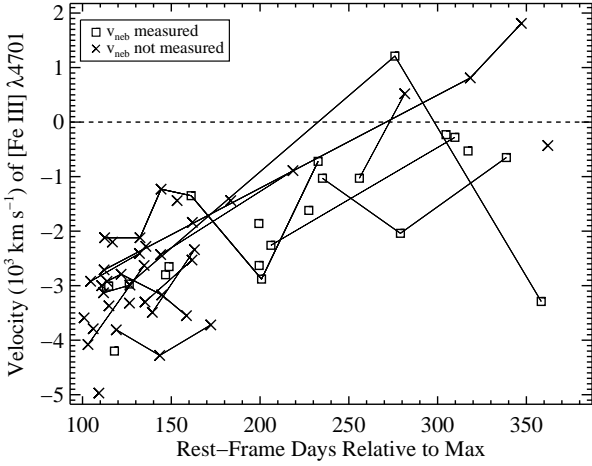


**Figure 4.** All velocities of [Fe III]  $\lambda 4701$  measured in this work. Solid lines connect multiple velocities of individual objects. Squares represent spectra for which we measured a nebular velocity;  $\times$  symbols represent spectra for which we did not.

cally by  $\sim 2000\text{--}4000 \text{ km s}^{-1}$  at  $t = 100 \text{ d}$  and the amount of blueshift decreases approximately linearly with time. This temporal evolution is quite slow, however, with a typical change in velocity of only  $\sim 10\text{--}20 \text{ km s}^{-1} \text{ d}^{-1}$ . The velocity of the [Fe III]  $\lambda 4701$  feature is uncorrelated with the nebular velocity and hence with the individual velocity of either [Fe II]  $\lambda 7155$  or [Ni II]  $\lambda 7378$ . Furthermore, the [Fe III]  $\lambda 4701$  velocity is also uncorrelated with the Si II  $\lambda 6355$  velocity and  $\dot{v}$ .

#### 4.2 [Fe II] $\lambda 7155$ and [Ni II] $\lambda 7378$

The individual velocities of the [Fe II]  $\lambda 7155$  and [Ni II]  $\lambda 7378$  features show a relatively large scatter at all epochs, which is reflected in the large range of calculated nebular velocities. The temporal velocity evolution of both features is even slower than that of the [Fe III]  $\lambda 4701$  feature, with typical changes of a few  $\text{km s}^{-1} \text{ d}^{-1}$ .

Since the average of the velocities of [Fe II]  $\lambda 7155$  and [Ni II]  $\lambda 7378$  is used to calculate  $v_{\text{neb}}$ , it is instructive to compare these two velocities with each other. The difference in these velocities has a relatively large scatter at all epochs, but we find no bias above or below zero velocity. The average *absolute* difference between the two velocities, however, is  $\sim 900 \text{ km s}^{-1}$ , which is reflected in our  $v_{\text{neb}}$  uncertainties discussed above. Despite this, the two velocities are highly correlated (Pearson coefficient of 0.84) and the difference between the two has a typical temporal evolution of  $< 10 \text{ km s}^{-1} \text{ d}^{-1}$ .

#### 4.3 Nebular Velocities

##### 4.3.1 Spectral Comparisons

Like the [Fe II]  $\lambda 7155$  and [Ni II]  $\lambda 7378$  velocities from which it is calculated, the nebular velocity does not change much with time (typical values being only a few  $\text{km s}^{-1} \text{ d}^{-1}$ , similar to what has been seen previously; e.g., Maeda et al. 2011). Furthermore, all four SNe Ia which have measured

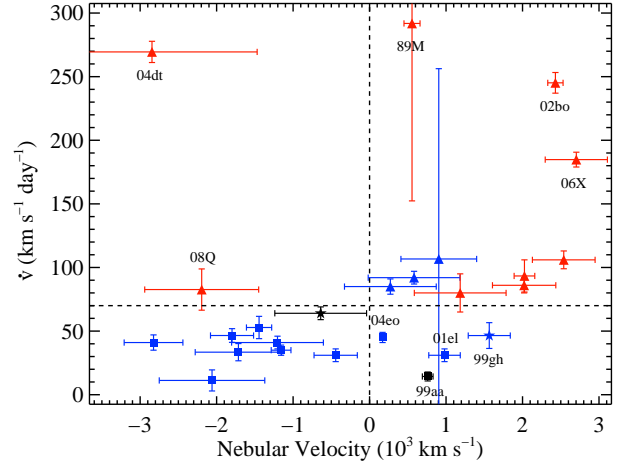


**Figure 5.** Nebular velocity versus velocity gradient. Shapes and colours of the data points are the same as in Figure 3. The vertical dashed line at  $0 \text{ km s}^{-1}$  separates blueshifted (left) and redshifted (right) nebular velocities. The horizontal dashed line at  $70 \text{ km s}^{-1} \text{ d}^{-1}$  separates LVG (below) and HVG (above) objects.

[Fe II]  $\lambda 7155$  and [Ni II]  $\lambda 7378$  velocities in multiple late-time spectra show no significant change in their nebular velocities with time (for  $130 < t < 360 \text{ d}$ ). Thus, a single measurement of  $v_{\text{neb}}$  appears to be sufficient to determine the typical nebular velocity of a given SN Ia.

Measurements of the velocity gradient were made for all objects with multiple near-maximum-brightness spectra in BSNIP, in Matheson et al. (2008), or in Blondin et al. (2012) (i.e., all SNe Ia listed in Table 2 except SNe 1993Z and 2003gs). The  $\dot{v}$  values calculated in this work are consistent at the  $2\sigma$  level with those found in previous studies (Benetti et al. 2005; Maeda et al. 2010a). We also plot previously published  $\dot{v}$  and  $v_{\text{neb}}$  values for 12 SNe Ia from Maeda et al. (2011) and Blondin et al. (2012).

Of the 25 objects with measured velocity gradients, 11 are LVG, 12 are HVG, and 2 are FAINT, which is similar to the distribution of types found by Maeda et al. (2010a), though they have a slightly larger fraction of LVG objects. Figure 5 presents these velocity-gradient measurements versus the nebular velocity; shapes and colours of the data points represent the Benetti and Wang types, respectively, as in Figure 3. The vertical dashed line at  $0 \text{ km s}^{-1}$  is the demarcation between blueshifted (left) and redshifted (right) nebular velocities; the horizontal dashed line at  $70 \text{ km s}^{-1} \text{ d}^{-1}$  is the demarcation between LVG (below) and HVG (above) objects.

Maeda et al. (2010a) found a correlation between  $v_{\text{neb}}$  and  $\dot{v}$ , and the BSNIP data support this conclusion, with some caveats. The Pearson coefficient for all of the data in Figure 5 is only 0.25 and the Spearman rank correlation coefficient is 0.39.<sup>2</sup> However, SN 2004dt was found to be somewhat peculiar (showing evidence for high-velocity and clumpy ejecta at early times; e.g., Altavilla et al. 2007) and

<sup>2</sup> This is perhaps the more appropriate value to examine here since the relationship appears to be nonlinear.

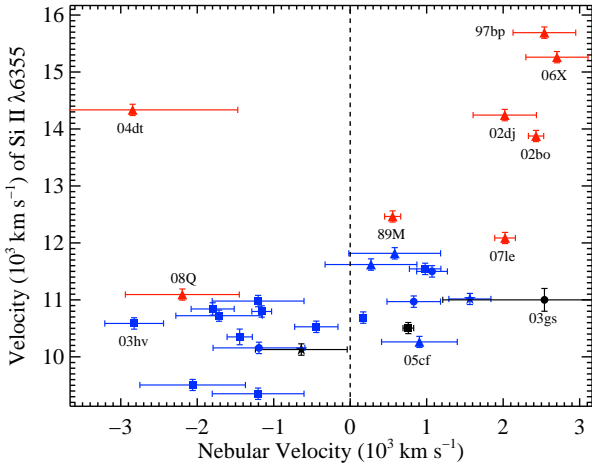


**Figure 6.** Nebular velocity versus Si II  $\lambda 6355$  velocity. Shapes and colours of the data points are the same as in Figure 3. Some of the outlying points are labeled. The vertical dashed line at  $0 \text{ km s}^{-1}$  separates blueshifted (left) and redshifted (right) nebular velocities.

did not follow the relationship of Maeda et al. (2010a). Also, there are only two BSNIP spectra of SN 1989M and they were obtained just 1 d apart, thus the lever arm for the  $\dot{v}$  calculation is small and the accuracy of the measurement is small (hence the large error bars for that data point).

Removing SN 2004dt (SNe 2004dt and 1989M) yields a Pearson correlation coefficient of 0.51 (0.62) and a Spearman rank correlation coefficient of 0.56 (0.59). This indicates that the nebular velocity is correlated with the velocity gradient, with the significance of the correlation at the  $2\sigma$  ( $3\sigma$ ) level. If we ignore SN 2004dt, all HVG objects have redshifted nebular lines, except SN 2008Q which is extremely close to the LVG/HVG border. We also find that nearly 3/4 of all LVG objects have blueshifted nebular spectral features. A Kolmogorov-Smirnov (KS) test on the nebular velocities of LVG and HVG objects implies that they very likely come from different parent populations ( $p \approx 0.016$ ). When removing SN 2004dt, the difference is even stronger ( $p \approx 0.007$ ).

The near-maximum-brightness Si II  $\lambda 6355$  velocity can also be compared to the nebular velocity for 14 of the SNe Ia in Table 2, as well as 15 SNe Ia from Maeda et al. (2011) and Blondin et al. (2012). We measure the Si II  $\lambda 6355$  velocity only in BSNIP spectra within 8 d of maximum brightness.<sup>3</sup> When multiple BSNIP spectra within 8 d of maximum exist for a given object, only the one closest to maximum brightness is used for the Si II  $\lambda 6355$  velocity measurement. The near-maximum-light velocities are plotted against the nebular velocities in Figure 6 with shapes and colours of data points the same as in Figure 3; the vertical dashed line separates blueshifted (left) and redshifted (right) nebular velocities.

A moderate correlation exists for all of the data pre-

sented in Figure 6 (Pearson and Spearman coefficients are both 0.51). If SN 2004dt is again ignored, a strong correlation exists (Pearson coefficient of 0.70 and Spearman coefficient of 0.64). Most HV objects have redshifted emission lines at late time, but normal-velocity objects have both blueshifted *and* redshifted nebular features. A KS test of the nebular velocities indicates, however, that the HV and normal-velocity objects do come from different parent populations ( $p \approx 0.021$  for all of the data and  $p \approx 0.009$  when ignoring SN 2004dt).

The overall trend and even the location of each object in the parameter space (given the measurement uncertainties) is quite similar to Figure 5. This is generally unsurprising given the results above involving the velocity gradient, since most (but not all) HV (normal-velocity) objects are also HVG (LVG) objects (Table 2 of Wang et al. 2006; Silverman et al. 2012d). Furthermore, the Si II  $\lambda 6355$  velocity at  $t = 0$  d (i.e.,  $v_0$ ) can be approximated from the velocity gradient and, as expected, these velocities at maximum brightness correlate in almost exactly the same manner as what is seen in Figure 6.

To investigate whether late-time observations of SNe Ia are related to the amount of circumstellar interaction a SN Ia undergoes, Förster et al. (2012) measured the EW of narrow absorption from Na I D and Ca II H&K in the host galaxies of SNe Ia and compared them to nebular velocities. Using 212 BSNIP spectra of the 15 objects listed in Table 2, we attempt to measure the EW of host-galaxy Na I D and Ca II H&K absorption. Even in the relatively low-resolution spectra of the BSNIP sample, we are able to measure Na I D absorption in all 15 SNe Ia and Ca II H&K absorption in 11 of them. The final EWs listed in the last two columns of Table 2 are the median of all EW measurements for each object (and the uncertainty is the standard deviation).

There are 6 objects in the current work that were also studied by Förster et al. (2012), and the EW measurements for all of these SNe Ia are consistent at the  $2\sigma$  level. In contrast to previous work (Förster et al. 2012), the BSNIP data do *not* show a significant correlation between the EWs of Na I D and Ca II H&K absorption. Förster et al. (2012) also found, at quite high significance, that objects with redshifted nebular velocities have larger EWs of Na I D and Ca II H&K absorption. They interpret this result as indicating that these objects have stronger circumstellar interaction or larger amounts of circumstellar material, and thus they claim that nebular velocities are directly related to SN Ia environments.

The objects with redshifted  $v_{\text{neb}}$  in BSNIP *tend* to have stronger absorption from Na I D and Ca II H&K, but this is not always the case, and the difference between objects with blueshifted and redshifted nebular velocities is not significant. Therefore, we are unable to confirm the findings of Förster et al. (2012) that the environments of SNe Ia directly affect nebular velocities (or vice versa).

#### 4.3.2 Photometric Comparisons

As mentioned above, the photometric parameters used in this work can be found in Ganeshalingam et al. (2010). Of the 15 objects listed in Table 2, 14 have near-maximum-brightness light curves which allow for the measurement of  $\Delta m_{15}(B)$ . We also analyse 17 additional objects from Maeda

<sup>3</sup> Spectra within 5 d of maximum brightness were used by Silverman et al. (2012d), but applying this constraint would remove three objects from the study of Si II  $\lambda 6355$  velocity versus nebular velocity.

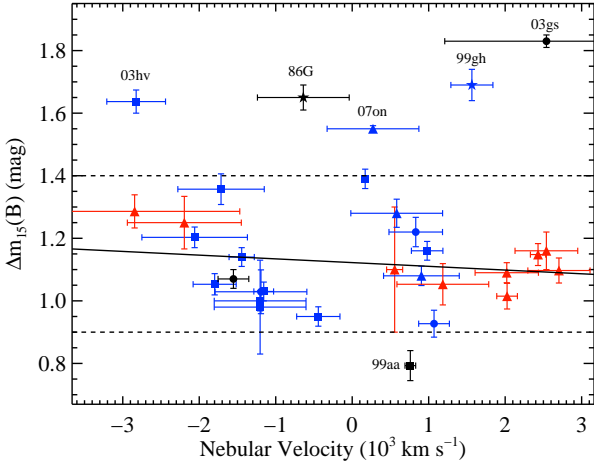


**Figure 7.** Nebular velocity versus  $\Delta m_{15}(B)$ . Shapes and colours of the data points are the same as in Figure 3. The six objects with  $\Delta m_{15}(B)$  values which fall outside the “normal” range ( $0.9 < \Delta m_{15}(B) < 1.4$  mag, denoted by the horizontal dashed lines) are labeled. The solid line is the linear fit to the data when ignoring these seven outliers.

et al. (2011) and Blondin et al. (2012). Most of them have  $0.9 < \Delta m_{15}(B) < 1.4$  mag, which represents the range of “normal” SNe Ia (e.g., Ganeshalingam et al. 2010). This range is denoted by the horizontal dashed lines in Figure 7, where we plot  $v_{\text{neb}}$  against  $\Delta m_{15}(B)$  and have labeled the six objects that fall outside the normal range of  $\Delta m_{15}(B)$  values.

When including all objects presented in the figure, the data are completely uncorrelated (Pearson correlation coefficient of  $-0.009$ ), similar to what has been seen previously (Blondin et al. 2012). Even when the six outliers (SNe 1986G, 1999aa, 1999gh, 2003gs, 2003hv, and 2007on) are ignored, there is still no significant evidence of a correlation between  $v_{\text{neb}}$  and  $\Delta m_{15}(B)$  (Pearson correlation coefficient of  $-0.16$ ). The solid line in Figure 7 is the linear fit to the data when ignoring these six outliers. Furthermore, the slope of this linear fit is consistent with zero, and it is clear that for a given  $\Delta m_{15}(B)$  there is a huge range of possible  $v_{\text{neb}}$  values. This result, which matches that of previous studies (Maeda et al. 2010a; Blondin et al. 2012), is illustrated in Figure 8, where the  $[\text{Fe II}] \lambda 7155$  and  $[\text{Ni II}] \lambda 7378$  features are plotted for three normal-luminosity objects all with  $\Delta m_{15}(B) \approx 1.1$  mag. The solid vertical lines represent the nebular velocity for both features of each object while the dotted vertical lines denote the rest wavelengths of the two features. Despite their nearly identical light curves, these three objects show significantly different nebular velocities with a range spanning  $\sim 4500$  km  $\text{s}^{-1}$ .

In Silverman et al. (2012c),  $(B - V)_{\text{max}}$  was defined as the observed  $B - V$  colour of the SN at  $B$ -band maximum brightness. In Figure 9 we plot  $v_{\text{neb}}$  versus  $(B - V)_{\text{max}}$  using this definition for the BSNIP data<sup>4</sup> as well as 14 additional SNe Ia from Maeda et al. (2011) and Blondin et al. (2012). In this parameter space there appears to be three outliers

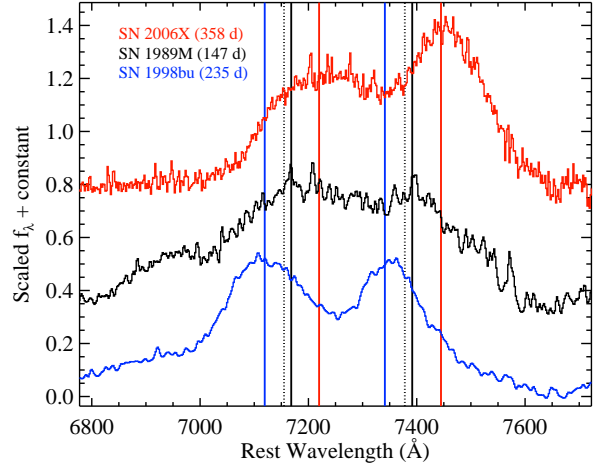


**Figure 8.** The deredshifted  $[\text{Fe II}] \lambda 7155$  and  $[\text{Ni II}] \lambda 7378$  features of SNe 2006X, 1989M, and 1998bu, all of which have  $\Delta m_{15}(B) \approx 1.1$  mag. The solid vertical lines are the nebular velocity for both features of each object, while the dotted vertical lines are the rest wavelengths of the two features.

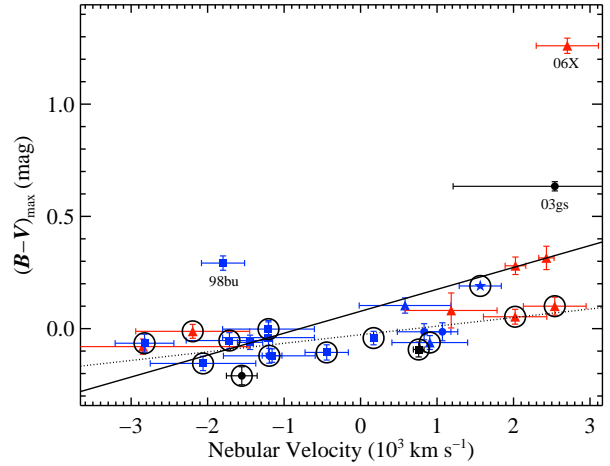


**Figure 9.** Nebular velocity versus observed  $(B - V)_{\text{max}}$ . Shapes and colours of the data points are the same as in Figure 3. Two of the labeled outliers (SNe 1998bu and 2006X) have significant reddening from their host galaxies, while the third labeled outlier (SN 2003gs) shows little host-galaxy reddening. The solid line is the linear fit to all of the data. The circled points are objects in the low-extinction sample and the dotted line is the linear fit to this subset.

(labeled in Figure 9). Two of these, SNe 1998bu and 2006X, are known to have substantial extinction from their host galaxies (e.g., Wang et al. 2008; Matheson et al. 2008). On the other hand, the third outlier (SN 2003gs) shows no evidence for significant host-galaxy extinction (Krisciunas et al. 2009).

Utilising all data in Figure 9,  $v_{\text{neb}}$  is found to be correlated (at the  $> 3\sigma$  level) with  $(B - V)_{\text{max}}$  (Pearson coefficient of 0.59), and the linear fit to these data is shown in the figure as the solid line. Blondin et al. (2012) found no correlation between  $v_{\text{neb}}$  and *intrinsic*  $B - V$  colour at  $B$ -

<sup>4</sup> SNe 1989M and 1993Z do not have colour information available.

band maximum for their full sample or when removing the peculiar SN 2004dt. However, they see a correlation similar to ours (with Pearson correlation coefficient of 0.82) for objects with  $v_{\text{neb}} > -2000 \text{ km s}^{-1}$ ; note that most of the objects presented herein also have  $v_{\text{neb}} > -2000 \text{ km s}^{-1}$ .

Since  $(B - V)_{\text{max}}$  is an *observed* SN colour (and thus a mixture of intrinsic SN colour and reddening from the host galaxy), we also investigate possible correlations between  $v_{\text{neb}}$  and  $(B - V)_{\text{max}}$  for various low-extinction subsets of our sample. Simply removing SN 2006X or both SNe 2006X and 1998bu from the analysis (since they are known to have large host-galaxy extinction) increases the Pearson coefficient to 0.60 and 0.77, respectively (and both correlations are significant at the  $\sim 3\sigma$  level). Concentrating only on objects with  $(B - V)_{\text{max}} < 0.2 \text{ mag}$ , we find a similarly strong correlation (Pearson coefficient of 0.64) again at the  $> 3\sigma$  level.

On the other hand, a low-extinction sample was defined by Blondin et al. (2012), and no correlation between  $v_{\text{neb}}$  and intrinsic  $(B - V)_{\text{max}}$  was detected. In this work we use similar criteria as Blondin et al. (2012) to define our low-extinction sample. A SN Ia is considered part of this sample if it resides in an E/S0 host galaxy, is found far (in projected distance) from a host galaxy of any type, or has a low value of  $A_V$  according to MLCS2k2 (Jha et al. 2007). Objects in the low-extinction sample are marked with a ‘†’ in Table 2 and are circled in Figure 9. In contrast to Blondin et al. (2012), we find a correlation between  $v_{\text{neb}}$  and observed  $(B - V)_{\text{max}}$  for the low-extinction sample (Pearson correlation coefficient of 0.63) at the  $\sim 2.5\sigma$  level, and the linear fit to this subset of SNe Ia is plotted in Figure 9 as a dotted line.

## 5 CONCLUSIONS

In this work we have analysed late-time ( $t > 100 \text{ d}$ ) optical spectra of low-redshift ( $z < 0.1$ ) SNe Ia which mostly come from the BSNIP dataset (Silverman et al. 2012a). The lone exception is SN 2011by, and we present and analyse 9 spectra of this object (2 of which are at late times). After removing objects that do not follow the Phillips relation (Phillips 1993) and spectra that do not cover either of the wavelength ranges of interest (namely the [Fe III]  $\lambda 4701$ , [Fe II]  $\lambda 7155$ , and [Ni II]  $\lambda 7378$  features), we are left with 34 SNe Ia with 60 spectra having  $t > 100 \text{ d}$ . Of these, 7 were studied by Maeda et al. (2010a), and those same 7 plus 2 more were studied by Blondin et al. (2012). We add to the BSNIP data nebular spectral feature measurements of 20 SNe Ia from previously published work (Maeda et al. 2011; Blondin et al. 2012). This sample represents the largest set of late-time SN Ia spectra ever analysed.

We attempted to measure the FWHM and velocity of the three nebular emission features mentioned above and are able to measure the [Fe III]  $\lambda 4701$  line in all late-time data discussed in this work. On the other hand, we are only able to calculate velocities of the [Fe II]  $\lambda 7155$  and [Ni II]  $\lambda 7378$  features in 22 spectra of 15 SNe Ia. To successfully measure these features it seems that the SN Ia should be spectroscopically normal, the spectrum should have  $S/N \gtrsim 20 \text{ px}^{-1}$ , and the spectrum should be older than  $\sim 160 \text{ d}$  past maximum brightness. Following Maeda et al. (2010a),

we calculate  $v_{\text{neb}}$  from the mean of the individual velocities of the [Fe II]  $\lambda 7155$  and [Ni II]  $\lambda 7378$  features.

The FWHM of [Fe III]  $\lambda 4701$  is anticorrelated with  $\Delta m_{15}(B)$ . However, if the 6 objects with  $\Delta m_{15}(B) > 1.6 \text{ mag}$  are removed, the correlation effectively disappears. The same results are found when using only spectra from 250–300 d past maximum brightness. Thus, this possible relationship seems to be driven solely by the most under-luminous SNe Ia. This feature is blueshifted by  $\sim 2000\text{--}4000 \text{ km s}^{-1}$  at  $t = 100 \text{ d}$ , and the amount of blueshift decreases approximately linearly with time. However, this temporal evolution is quite slow, with a typical change in velocity of only  $\sim 10\text{--}20 \text{ km s}^{-1} \text{ d}^{-1}$ .

The nebular velocity likewise does not change much with time (typical values are a few  $\text{km s}^{-1} \text{ d}^{-1}$ ). Furthermore, the BSNIP data weakly support the finding of Maeda et al. (2010a) that  $v_{\text{neb}}$  and  $\dot{v}$  are correlated. Nearly all HVG objects have redshifted nebular lines and most LVG objects have blueshifted nebular spectral features. A similar result is found when using the near-maximum-brightness velocity instead of the velocity gradient and assuming HV (normal-velocity) objects are also HVG (LVG) objects (which is a reasonable assumption, e.g., Silverman et al. 2012d). The data studied in this work also show no significant correlation between the EWs of Na I D or Ca II H&K absorption and  $v_{\text{neb}}$ ; thus, we are unable to confirm previous claims that the environments of SNe Ia directly affect nebular velocities, or vice versa (Förster et al. 2012). No significant correlation is found between  $v_{\text{neb}}$  and  $\Delta m_{15}(B)$ , and SNe Ia with nearly identical light curves can have a wide range of nebular velocities, spanning  $\sim 4500 \text{ km s}^{-1}$  in Figure 8. Our data also indicate a correlation between observed  $(B - V)_{\text{max}}$  and  $v_{\text{neb}}$ .

Although the combined dataset analysed in this work constitutes the largest late-time SN Ia spectral dataset ever studied, it still contains only a handful of objects. The analysis herein could certainly be improved and extended by obtaining more nebular SN Ia spectra. While BSNIP (and the CfA, Blondin et al. 2012) has gathered, published, and analysed their SN Ia spectral data, larger transient searches such as the Palomar Transient Factory (PTF; Rau et al. 2009; Law et al. 2009) and Pan-STARRS (Kaiser et al. 2002) will be able to add significantly to the number of late-time SN Ia spectra.

## ACKNOWLEDGMENTS

We would like to thank G. Canalizo, S. B. Cenko, K. Clubb, M. Cooper, A. Diamond-Stanic, E. Gates, K. Hiner, M. Kandrashoff, M. Lazaro, A. Miller, P. Nugent, and the overall LAMP collaboration (Barth et al. 2011) for their help with the observations of SN 2011by. R. J. Foley and S. W. Jha discussed earlier drafts of this work with us, and the anonymous referee provided comments and suggestions that improved the manuscript. We are grateful to the staffs at the Lick and Keck Observatories for their support. Some of the data utilised herein were obtained at the W. M. Keck Observatory, which is operated as a scientific partnership among the California Institute of Technology, the University of California, and NASA; the observatory was made possible by the generous financial support of the W. M. Keck Foundation. The authors wish to recognise and acknowledge the

very significant cultural role and reverence that the summit of Mauna Kea has always had within the indigenous Hawaiian community; we are most fortunate to have the opportunity to conduct observations from this mountain. This work is supported by NSF grants AST-0908886 and AST-1211916, DOE grants DE-FC02-06ER41453 (SciDAC) and DE-FG02-08ER41563, the TABASGO Foundation, and the Christopher R. Redlich Fund. J.M.S. is grateful to Marc J. Staley for a Graduate Fellowship. KAIT and its ongoing operation were made possible by donations from Sun Microsystems, Inc., the Hewlett-Packard Company, AutoScope Corporation, Lick Observatory, the NSF, the University of California, the Sylvia & Jim Katzman Foundation, and the TABASGO Foundation. We dedicate this paper to the memory of Wallace L. W. Sargent (deceased 2012 Oct. 29); the discovery of SN 1985F by Filippenko & Sargent (1985) sparked A.V.F.'s intense interest in supernovae and dramatically affected his career.

## REFERENCES

- Aldering G., et al., 2006, *ApJ*, 650, 510  
 Altavilla G., et al., 2007, *A&A*, 475, 585  
 Amanullah R., et al., 2010, *ApJ*, 716, 712  
 Astier P., et al., 2006, *A&A*, 447, 31  
 Barth A. J., et al., 2011, *ApJ*, 743, L4  
 Benetti S., et al., 2005, *ApJ*, 623, 1011  
 Blondin S., et al., 2012, *AJ*, 143, 126  
 Blondin S., Tonry J. L., 2007, *ApJ*, 666, 1024  
 Cappellaro E., et al., 2001, *ApJ*, 549, L215  
 Chornock R., Filippenko A. V., Branch D., Foley R. J., Jha S., Li W., 2006, *PASP*, 118, 722  
 Colgate S. A., McKee C., 1969, *ApJ*, 157, 623  
 Conley A., et al., 2011, *ApJS*, 192, 1  
 Filippenko A. V., et al., 1992a, *ApJ*, 384, L15  
 Filippenko A. V., et al., 1992b, *AJ*, 104, 1543  
 Filippenko A. V., Li W. D., Treffers R. R., Modjaz M., 2001, in Paczyński B., Chen W. P., Lemme C., eds, *Small-Telescope Astronomy on Global Scales*. Vol. 246, *Astron. Soc. Pac.*, San Francisco, p. 121  
 Filippenko A. V., Sargent W. L. W., 1985, *Nature*, 316, 407  
 Foley R. J., et al., 2012, *ApJ*, 744, 38  
 Förster F., González-Gaitán S., Anderson J., Marchi S., Gutiérrez C., Hamuy M., Pignata G., Cartier R., 2012, *ApJ*, 754, L21  
 Ganeshalingam M., et al., 2010, *ApJS*, 190, 418  
 Garavini G., et al., 2004, *AJ*, 128, 387  
 Hicken M., Wood-Vasey W. M., Blondin S., Challis P., Jha S., Kelly P. L., Rest A., Kirshner R. P., 2009, *ApJ*, 700, 1097  
 Hillebrandt W., Niemeyer J. C., 2000, *ARA&A*, 38, 191  
 Howell D. A., 2011, *Nature Communications*, 2  
 Hoyle F., Fowler W. A., 1960, *ApJ*, 132, 565  
 Immler S., Russell B. R., 2011, *ATel*, 3410, 1  
 Jha S., Branch D., Chornock R., Foley R. J., Li W., Swift B. J., Casebeer D., Filippenko A. V., 2006, *AJ*, 132, 189  
 Jha S., Riess A. G., Kirshner R. P., 2007, *ApJ*, 659, 122  
 Jin Z., Gao X., 2011, *CBET*, 2708, 1  
 Kaiser N., et al., 2002, in Tyson J. A., Wolff S., eds, *Proceedings of the Society of Photo-Optical Instrumentation Engineers (SPIE) Conference*. Vol. 4836. p. 154  
 Kessler R., et al., 2009, *ApJS*, 185, 32  
 Krisciunas K., et al., 2009, *AJ*, 138, 1584  
 Law N. M., et al., 2009, *PASP*, 121, 1395  
 Leibundgut B., et al., 1993, *AJ*, 105, 301  
 Leloudas G., et al., 2009, *A&A*, 505, 265  
 Li W., et al., 2000, in Holt S. S., Zhang W. W., eds, *Cosmic Explosions*. American Institute of Physics, New York, p. 103  
 Li W., et al., 2001, *PASP*, 113, 1178  
 Li W., et al., 2003, *PASP*, 115, 453  
 Li W., Filippenko A. V., Treffers R. R., Riess A. G., Hu J., Qiu Y., 2001, *ApJ*, 546, 734  
 Maeda K., et al., 2010a, *Nature*, 466, 82  
 Maeda K., et al., 2011, *MNRAS*, 413, 3075  
 Maeda K., Taubenberger S., Sollerman J., Mazzali P. A., Leloudas G., Nomoto K., Motohara K., 2010b, *ApJ*, 708, 1703  
 Matheson T., et al., 2008, *AJ*, 135, 1598  
 Mazzali P. A., Cappellaro E., Danziger I. J., Turatto M., Benetti S., 1998, *ApJ*, 499, L49  
 Mazzali P. A., Hachinger S., 2012, *MNRAS*, 424, 2926  
 Miller J. S., Stone R. P. S., 1993, *Lick Obs. Tech. Rep.* 66. Santa Cruz: Lick Obs.  
 Nomoto K., Thielemann F.-K., Yokoi K., 1984, *ApJ*, 286, 644  
 Nugent P. E., et al., 2011, *Nature*, 480, 344  
 Oke J. B., Cohen J. G., Carr M., et al., 1995, *PASP*, 107, 375  
 Perlmutter S., et al., 1999, *ApJ*, 517, 565  
 Phillips M. M., 1993, *ApJ*, 413, L105  
 Phillips M. M., et al., 2007, *PASP*, 119, 360  
 Phillips M. M., Wells L. A., Suntzeff N. B., Hamuy M., Leibundgut B., Kirshner R. P., Foltz C. B., 1992, *AJ*, 103, 1632  
 Pooley D., 2011, *ATel*, 3456, 1  
 Prieto J. L., et al., 2007, *arXiv: 0706.4088*  
 Rau A., et al., 2009, *PASP*, 121, 1334  
 Riess A. G., et al., 1998, *AJ*, 116, 1009  
 Riess A. G., et al., 2007, *ApJ*, 659, 98  
 Savitzky A., Golay M. J. E., 1964, *Analytical Chemistry*, 36, 1627  
 Schmidt B. P., et al., 1994, *ApJ*, 434, L19  
 Silverman J. M., et al., 2012a, *MNRAS*, 425, 1789  
 Silverman J. M., et al., 2012b, *ApJ*, 756, L7  
 Silverman J. M., Ganeshalingam M., Li W., Filippenko A. V., 2012c, *MNRAS*, 425, 1889  
 Silverman J. M., Ganeshalingam M., Li W., Filippenko A. V., Miller A. A., Poznanski D., 2011, *MNRAS*, 410, 585  
 Silverman J. M., Kong J. J., Filippenko A. V., 2012d, *MNRAS*, 425, 1819  
 Stanishev V., et al., 2007, in di Salvo T., et al., eds, *The Multicolored Landscape of Compact Objects and Their Explosive Origins*. Vol. 924 of *American Institute of Physics Conference Series*, pp 336–341  
 Stritzinger M., Mazzali P. A., Sollerman J., Benetti S., 2006, *A&A*, 460, 793  
 Stritzinger M., Sollerman J., 2007, *A&A*, 470, L1  
 Strolzer L., et al., 2002, *AJ*, 124, 2905

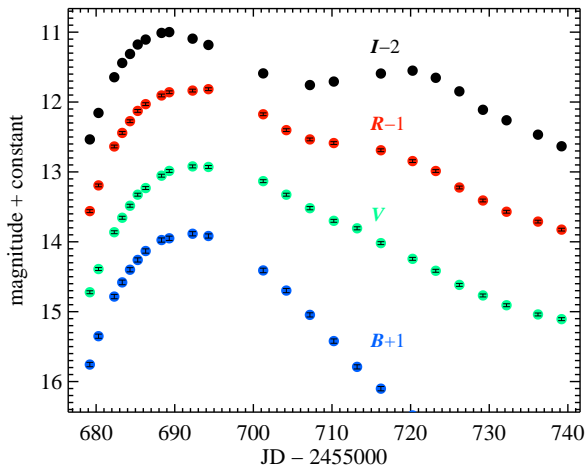


**Figure A1.** *BVRI* light curves of SN 2011by from KAIT.

- Suntzeff N., Candia P., Stritzinger M., 2003, IAU Circ., 8171, 1  
 Suzuki N., et al., 2012, ApJ, 746, 85  
 Wang L., Baade D., Höflich P., Wheeler J. C., Kawabata K., Khokhlov A., Nomoto K., Patat F., 2006, ApJ, 653, 490  
 Wang X., et al., 2008, ApJ, 675, 626  
 Wang X., et al., 2009, ApJ, 699, L139  
 Wang X., Li W., Filippenko A. V., Foley R. J., Smith N., Wang L., 2008, ApJ, 677, 1060  
 Wood-Vasey W. M., et al., 2007, ApJ, 666, 694  
 Zhang T., Zhou Z., Wang X., 2011, CBET, 2708, 3

## APPENDIX A: OBSERVATIONS OF SN 2011BY

SN 2011by was discovered by Jin & Gao (2011) on 2011 Apr. 26.8 UT in NGC 3972 with J2000.0 coordinates  $\alpha = 11^{\text{h}}55^{\text{m}}45.56^{\text{s}}$ ,  $\delta = +55^{\circ}19'33''.8$ , and it was classified  $\sim 1$  d after discovery as a young SN Ia by Zhang et al. (2011). Immler & Russell (2011) detected X-ray emission coincident with SN 2011by  $\sim 40$  d after discovery using *Swift*/XRT, but the emission was found to be unassociated with the SN using *Chandra* observations taken  $\sim 3$  weeks later (Pooley 2011).

Broad-band *BVRI* photometry of SN 2011by was obtained using the 0.76-m Katzman Automatic Imaging Telescope (KAIT) at Lick Observatory (Li et al. 2000; Filippenko et al. 2001) and is shown in Figure A1. The data were reduced using standard procedures, the details of which can be found in Ganeshalingam et al. (2010). The optical light curves of SN 2011by indicate that it reached *B*-band maximum brightness on 2011 May 9.9 UT and that it had  $\Delta m_{15}(B) = 1.14 \pm 0.03$  mag.

We obtained 7 near-maximum-brightness spectra of SN 2011by using the Lick/Kast double spectrograph. They span  $\sim 12$  d before to  $\sim 15$  d after maximum brightness, as shown in the top panel of Figure A2. In addition, we used Keck/LRIS to acquire 2 late-time spectra at 206 and 310 d past maximum (shown in the bottom panel of Figure A2), the spectral feature measurements of which can be found at

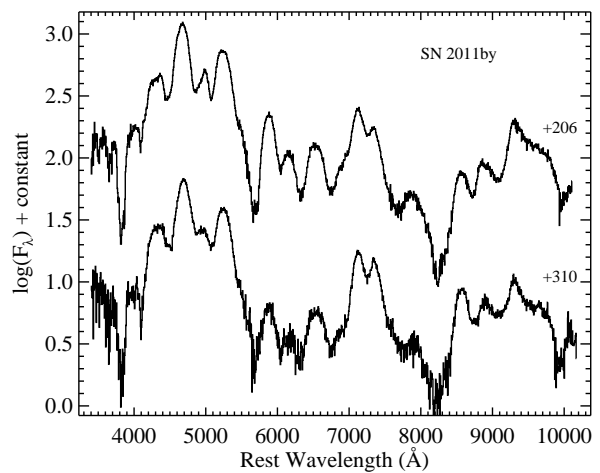
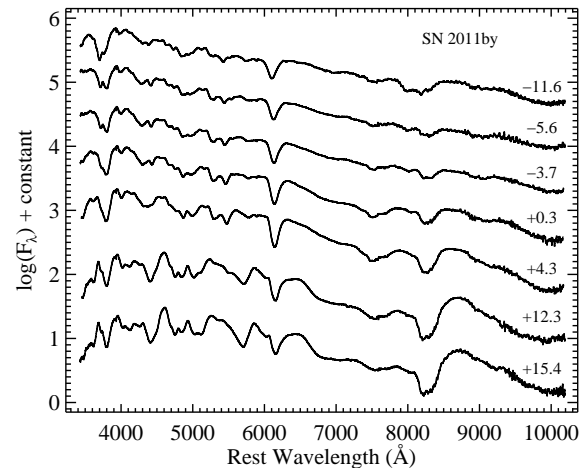


**Figure A2.** Near-maximum-brightness (*top*) and late-time (*bottom*) spectra of SN 2011by, labeled with age relative to the time of maximum brightness. The data have had their host-galaxy recession velocity removed and have been corrected for Galactic reddening.

the end of Table 1. Details of all of our spectral observations of SN 2011by can be found in Table A1.

Consistent with the light curves, the spectra indicate that this object is quite normal; the SuperNova IDentification code (SNID; Blondin & Tonry 2007), as implemented by Silverman et al. (2012a), was run on all of our spectra of SN 2011by and it is definitively classified as spectroscopically normal. As in Silverman et al. (2012d), we calculated the near-maximum-brightness velocity based on the minimum of the Si II  $\lambda 6355$  absorption feature and find that it shows a “normal” velocity near maximum brightness, as opposed to some SNe Ia which exhibit higher-than-average expansion velocities (e.g., Wang et al. 2009). Furthermore, since we have multiple spectra near maximum brightness, we can calculate the velocity gradient (e.g., Benetti et al. 2005); SN 2011by falls squarely in the LVG group.

Individual objects (some found by amateur astronomers and some by large-scale surveys) discovered in nearby galaxies soon after explosion will be invaluable resources for extending our understanding of SNe Ia. SN 2011by represents

**Table A1.** Journal of spectroscopic observations of SN 2011by.

UT Date	Age <sup>a</sup>	Range (Å)	Airmass <sup>b</sup>	Exp (s)
2011 Apr. 28.2	−11.6	3440–10200	1.05	600
2011 May 4.2	−5.6	3440–10200	1.06	600
2011 May 6.2	−3.7	3440–10200	1.05	600
2011 May 10.2	0.3	3438–10196	1.06	600
2011 May 14.2	4.3	3456–10200	1.07	600
2011 May 22.3	12.3	3464–10200	1.15	600
2011 May 25.3	15.4	3436–10200	1.27	600
2011 Dec. 2.6 <sup>c</sup>	206	3400–10138	1.50	450
2012 Mar. 15.5 <sup>c</sup>	310	3400–10200	1.32	900

<sup>a</sup>Rest-frame days relative to the date of *B*-band maximum brightness, 2011 May 9.9 (see Section 2.1).

<sup>b</sup>Airmass at midpoint of exposure.

<sup>c</sup>These observations used LRIS (Oke et al. 1995) on the 10-m Keck I telescope. The others used the Kast spectrograph on the Lick 3-m Shane telescope (Miller & Stone 1993).

an exquisite case study for the current work. In recent years there have been a handful of other nearby SNe Ia found soon after explosion (e.g., Nugent et al. 2011; Foley et al. 2012; Silverman et al. 2012b) that will also serve as excellent individual case studies once late-time spectra have been obtained and analysed.